Natural rubber/boehmite nanocomposites via latex compounding

Berki P., Khang D. Q., Tung N. T., Hai L. N., Czigány T., Karger-Kocsis J.

Accepted for publication in IOP Conference Series: Materials Science and Engineering
Published in 2018
DOI: 10.1088/1757-899X/426/1/012006

IOP Conf. Series: Materials Science and Engineering **426** (2018) 012006 doi:10.1088/1757-899X/426/1/012006

Natural rubber/boehmite nanocomposites *via* latex compounding

P Berki[1], D Q Khang[2], N T Tung[2], L N Hai[3], T Czigány[1,4] and J Karger-Kocsis[1,4*]

[1] Department of Polymer Engineering, Faculty of Mechanical Engineering, Budapest University of Technology and Economics, Budapest, Hungary
[2] Department of Functional Polymers and Nanomaterials, Institute of Chemistry, Vietnam Academy of Science and Technology, Hanoi, Vietnam
[3] Department of Chemical Technology Development, Center for High Technology Development, Vietnam Academy of Science and Technology, Hanoi, Vietnam
[4] MTA-BME Research Group of Composite Science and Technology, Budapest, Hungary

E-mail: karger@pt.bme.hu

Abstract. Natural rubber (NR) latex was modified with unmodified boehmite alumina (BA) nanoparticles, added in NR up to 15 parts per hundred rubber (phr) amounts. Dispersion of the BA nanofillers was inspected in scanning electron microscopy (SEM). The tensile and fracture mechanical (J-integral approach) properties of the NR/BA nanocomposites were determined. Information on the rubber-BA and possible BA-BA interactions were deduced from dynamic mechanical analysis (DMA) and differential scanning calorimetric (DSC) tests. It was found that BA particles, through agglomerated, were well dispersed in the NR/BA nanocomposites up to a given threshold (7.5 phr). Improvements in the tensile (strength) and fracture mechanical properties (crack initiation- and propagation-related data) were found until this threshold BA content. DMA results confirmed enhanced stiffness and Payne-effect with increasing BA content both in the glassy and rubbery states and in the rubbery state, respectively. The amount of the bound NR fraction on the BA surface was rather small according to DSC results. It was thus concluded that unmodified BA acts as a semi-active nanofiller in NR.

1. Introduction

Nanocomposites can be easily produced using polymer latices and water swellable, water dispersible nanofillers. Note that polymer latex is an aqueous dispersion of nano-scaled polymer particles. Among the water swellable and dispersible nanofillers clays (of natural or synthetic origin), oxidized carbonaceous nanofillers (carbon nanotube, nanofiber, graphene), nanocellulose and boehmite should be mentioned. These nanofillers have been introduced in various thermoplastics *via* water-assisted compounding versions [1]. Many reports are available also on clay-containing thermoplastics making use of this technique [1]. Moreover, works were published also boehmite alumina (BA) filled nanocomposites using various thermoplastic matrices [2]. Introduction of aqueous dispersion of nanocellulose particles, whiskers is preferably combined with plasticization to produce thermoplastic starch [3]. The basic reason of the successful preparation of thermoplastic nanocomposites with clays and BAs through water-mediated melt compounding is that the concentration of these nanofillers in their aqueous dispersions may be as high as 10 wt%. This is highly beneficial for the fast evaporation of the

water carrier during extrusion compounding based on the fact that the target nanofiller content in the related thermoplastic is at about 3 wt.% [1]. The water-mediated melt compounding technique is less suited for oxidized graphene, oxidized carbon nanotube, and the like, because their concentration in aqueous fluids is usually below 1 wt.% [4].

The introduction of the above mentioned nanofillers in rubber latices is straightforward because it is not concentration-dependent since the dispersing fluid for the nanofillers is the latex itself. Large body of works addressed the preparation of rubber nanocomposites *via* latex compounding, also referred to latex cocoagulation. As rubber latices mostly natural rubber (NR) and styrene-butadiene rubber (SBR), whereas as fillers clays [5, 6] and graphene oxide [7] were selected. Works published on NR/clay [5-6] and NR/graphene oxide [7, 8] nanocomposites, produced by the latex route, revealed a fine and homogenous dispersion of these nanofillers in the NR. The related dispersion was better than by traditional melt compounding [9]. This was associated with strong improvements in the mechanical properties compared to reference mixes produced by traditional melt compounding.

Boehmite aluminas (BAs) are oxide-hydroxides of aluminum, available in different shapes. BA may have very high specific surface area (>300 m^2/g) since the primary crystallite size may be as small as 4.5 nm which makes it ideal as a nanofiller for polymers [3]. The numerous hydroxyl groups on their surfaces guarantee the dispersion in aqueous fluids. The particle size of BA dispersed in aqueous media is, however, 4 to 10 times of its primary crystallite size. BAs with and without surface modifications were already incorporated in various thermoplastics and thermosets, as reviewed recently [3]. The modification of rubbers by BA is far less advanced compared to the companion thermoplastic- and thermoset-based nanocomposites. This is a surprising fact because many properties of BAs are in favour of application in rubbers. These features are: high specific surface (comparable to traditional fillers, such as carbon black and silica), different shapes (aspect ratios), surface basicity (unlike acidity, it does not influence the vulcanization substantially), versatile surface modification (to tailor the interfacial adhesion) and nanoscale dispersion in aqueous media (the possibility of using latex (pre)compounding). Researchers made use of various surface modification strategies of BA in works performed on rubber/BA nanocomposites [3]. By contrast, unmodified (pristine) BA was very rarely used as nanofiller for rubbers, and only one report is found for adopting the BA (though surface-modified) dispersion rubber latex [10].

Considering the above information our intention was to check whether the latex compounding method is applicable for the production of rubber/BA nanocomposites. In this work commercial BA was added in 0, 2.5, 5, 7.5, 10 and 15 parts per hundred rubber (phr) amounts to modify an NR latex that was coagulated and cured by sulfuric curatives. The microdispersion of the BA was studied by scanning electron microscopy. Properties of the NR/BA nanocomposites were assessed in dynamic mechanical thermal analysis, tensile and fracture mechanical (J-integral) tests. Differential scanning calorimetry served to estimate the bound (also termed to immobilized) NR fraction.

2. Experimental

2.1. Materials

Synthetic boehmite alumina (Disperal® 40) was kindly provided by Sasol Germany (Hamburg, Germany). Characteristics of this BA are: Al2O3 content 80 %, BET surface area: 100 m2/g, primary crystallite (120) size: 40 nm. NR latex with 60 wt. % dry content was purchased from Tay Ninh Rubber Company (Vietnam). The other chemicals such as sulfur (S) from Sae Kwang Chemicals Ind., Co. Ltd (South Korea), zinc oxide (ZnO) from Triveni Chemicals Company (India), stearic acid from PT Cisadane Raya Chemicals (Indonesia), dibenzothiazyl disulfide (DM), 2-benzothiazosulfenamide (CBS), polymerized 2,2,4-trimethyl-1,2-dihydroquinoline from TMQ, Kemai Chemicals Co. Ltd, (China), ethanol 96% v/v from Thinh Cuong Co. Ltd, (Vietnam) were used as received. NH3 solution (25%) was purchased from Guangdong Guanghua Sci.-Tech Co, Ltd. (China).

2.2. Preparation of the samples

Firstly, BA in different amounts was dispersed in distilled water setting a weight ratio of BA:H_2O = 1:15 by adding of NH_3 solution (25%) to adjust the pH of BA dispersion to pH = 10. The BA dispersion was stirred for 30 min by magnetic stirrer. Afterward, BA solution was further homogenised by sonication for 2 h to get a well-dispersed BA solution. Then, 60 ml NR latex was poured to the BA solution under magnetic stirring of 800 rpm and the mixing time was 1 h. Afterward, NR/BA nanocomposites were coagulated by adding ethanol and then washed with distilled water. Finally, NR/BA nanocomposites were dried in vacuum at room temperature for 1 day.

The latex precompounded NR/BA samples were mixed with sulfur, ZnO, SA, DM, CBS, TMQ according to the recipe in Table 1 on a laboratory two roll mill (Toyoseiki, Tokyo, Japan) at room temperature for 15 min. The samples were cured in a press (Toyoseiki, Tokyo, Japan) at 145 oC and 2 MPa pressure for 15 min producing sheets with 2 mm thickness.

Table 1. Designation and composition of the NR/BA mixes

Designation	Composition [phr]							
	NR latex (dried)	ZnO	Stearic acid	TMQ	CBS	Sulfur	DM	Boehmite (BA)
NR ref	100	5	1	1	1.5	2	0.5	-
NR-2.5BA	100	5	1	1	1.5	2	0.5	2.5
NR-5BA	100	5	1	1	1.5	2	0.5	5
NR-7.5BA	100	5	1	1	1.5	2	0.5	7.5
NR-10BA	100	5	1	1	1.5	2	0.5	10
NR-15BA	100	5	1	1	1.5	2	0.5	15

2.3. Characterization and testing

To get information on the BA dispersion in the NR the fracture surfaces of the nanocomposites were inspected in field-emission and scanning electron microscopes (FE-SEM: Hitachi S-4800, Tokyo, Japan and SEM: JEOL JSM 6380LA, Tokyo, Japan), respectively.

Tensile tests were performed on a Gotech AI 7000M (Taichung,Taiwan) machine at room temperature with crosshead speed 200 mm/min according to DIN 53504. The hardness of the specimens was measured by a Teclock JIS K7215A (TTS, Osaka, Japan) instrument.

Fracture mechanical tests were performed on single edge-notched tensile loaded (SEN-T) specimens. SEN-T specimens of 100 x 25 x 2mm dimension (length x width x thickness) with 10 mm initial notch length were loaded with 10 mm/min crosshead speed on the above mentioned Zwick testing machine. The crack tip opening displacement (CTOD) was followed by visual inspection using a digital miscroscope (Celestron 44302, USA). The camera was positioned in front of the crack in order to focus on the internal surface generated by blunting and/or growing of the crack. Prior to this test the crack surfaces were coated by talc for contrast. By analyzing the registered sequence of pictures the point where fracture started to propagate could be detected and the corresponding J-integral (J-critical) value determined by [11]:

$$J = \frac{\eta \cdot U}{t \cdot (W - a)} \quad (1)$$

where η is a geometry factor (0.9 in this case), U is the input energy (given by the area under the load-displacement curve up to the point considered), t is the thickness (≈ 2 mm), W is the width (25 mm) of the specimen and a is the initial crack length (10 mm). The J-integral was determined as a function of the crack tip opening displacement (CTOD) between 0.1 and 0.8 mm. J-critical was read at CTOD=0.1 mm, whereas the tearing modulus (T_J) was given by the slope of the linear regression fitted for the J vs CTOD data.

Dynamic-mechanical analysis (DMA) traces were registered on rectangular specimens in tensile mode at a static preload of 0.1 N with a superimposed sinusoidal 0.1% strain. The frequency was 10 Hz and the spectra were taken in a temperature range of -100 to 60 °C using a Q800 device of TA

Instruments (New Castle, DE, USA). The temperature ramp was 3°C/min. The DMA technique was used also to assess the Payne effect. It was determined in tensile mode at 30 °C using 10 Hz frequency and 0.01 N static preload with strain sweep from 0.01 to 10% strain (denoted as M0.01 and M10, respectively).

Differential scanning calorimetry (DSC) served to investigate the glass transition region of the neat and BA-containing NR systems. 3-5 mg samples were heated from -90 °C to room temperature at a rate of 5°C/min under nitrogen flushing in a Q2000 device of TA Instruments (New Castle, DE, USA). Change in the heat capacity was used to estimate the immobilized NR faction (see later).

3. Results and discussion

3.1. Particle characteristics

Figure 1 shows SEM pictures taken from the fracture surface of the NR nanocomposites containing 2.5 (NR-2.5BA) and 7.5 phr BA (NR-7.5BA), respectively. One can clearly see the average dispersed size of the BA agglomerates did not change significantly with the BA content, at least until 7.5 phr content. The size of the BA agglomerates is in the range of 200-300 nm. This range agrees very well with that of the Sasol's brochure (180-250 nm), measured in slightly acidic aqueous dispersion. A closer look on the BA agglomerates reveals even the presence of prismatic primary crystallites of low aspect ratio.

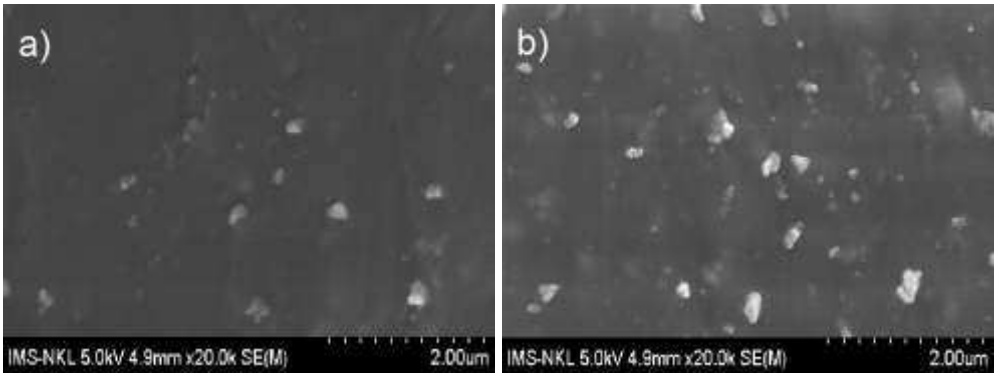

Figure 1. FE-SEM images showing the BA particles' dispersion in the NR-2.5BA (a) and NR-7.5BA (b) nanocomposites.

3.2. Mechanical and fracture mechanical properties

The mechanical (hardness, tensile strength, elongation at break) and fracture mechanical (J-critical, tearing modulus) of the unfilled (reference) NR and NR/BA nanocomposites are presented in Table 2.

The hardness increased monotonously with increasing amount of BA. The tensile strength went through a maximum (peaked at 7.5 phr) as a function of the nanofiller content suggesting agglomeration phenomena at high filler contents. The elongation at break decreased monotonously with the BA content. This is a usual feature when the amount of nanofillers is enhanced. The courses of J-critical and T_J as a function of the BA content were identical with that of the tensile strength, even the peak values at 7.5 phr BA agreed. This finding suggests that the dispersion of BA strongly affects both the J-critical and T_J. Inhomogeneous dispersion of BA particles owing to highly different agglomerates' sizes, associated with different matrix ligaments between them, facilitate the crack tip opening and growth.

Table 2. Mechanical and fracture mechanical properties of the NR/BA systems studied

Designation	Hardness [Sh °A]		Tensile strength [MPa]		Tensile strain [%]		J-critical [kJ/m^2]		Tearing modulus, T_J [MJ/m^3]	
NR ref	40	±1	19.01	±1.11	778	±20	3.85	±0.24	12.14	±0.78
NR-2.5BA	42	±1	25.82	±0.95	743	±15	5.11	±0.31	16.29	±0.81
NR-5BA	45	±1	27.80	±0.52	736	±19	6.21	±0.32	18.26	±0.66
NR-7.5BA	47	±1	29.53	±0.39	722	±21	6.82	±0.27	20.01	±0.55
NR-10BA	50	±1	24.70	±0.59	669	±34	6.58	±0.37	17.74	±0.76
NR-15BA	54	±1	20.90	±0.85	632	±32	5.19	±0.42	14.23	±0.82

3.3. Dynamic mechanical analysis

The storage modulus (E') vs. temperature and mechanical loss factor (tanδ) vs. temperature curves are depicted for the NR/BA nanocomposites in Figure 2.

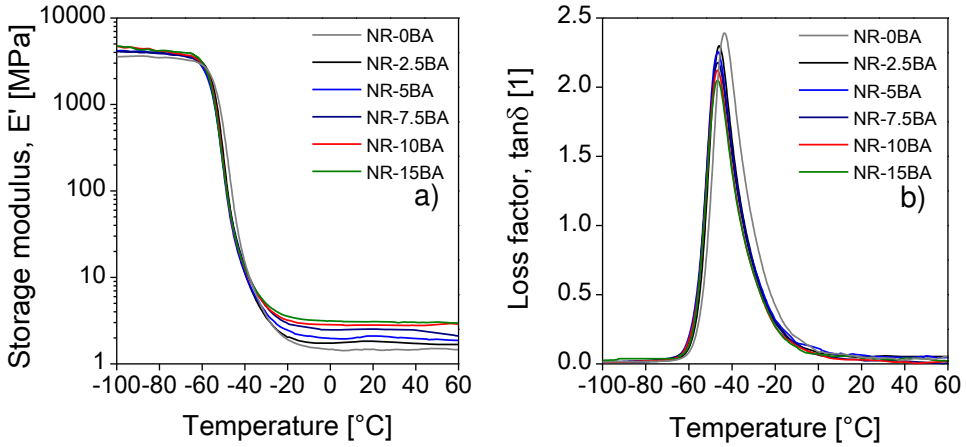

Figure 2. Storage modulus vs. temperature (a) and mechanical loss factor (tanδ) vs. temperature (b) curves for the NR/BA nanocomposites studied

One can notice in Figure 2a that both the glassy and rubbery moduli increased with increasing BA content. They were read at T_g-30 °C and T_g+30 °C, respectively (Table 3). This confirms the reinforcing effect of BA. The most surprising effect is that the tanδpeak was only slightly reduced with increasing amount of BA (cf. Figure 2b and Table 3). Modulus increase, reflecting the reinforcing effect, is usually associated with prominent decrease in the mechanical loss factor. Note that the glass transition temperature (T_g) values of the nanocomposites, determined as the peak temperature of tanδ, were slightly shifted toward lower temperatures (cf. Table 3). This was also unexpected and hints along with the high T_g peak values for a weak interphase. From the rubbery E'-moduli, read at the apparent mean molecular weight between crosslinks (M_c) was determined by the rubber elasticity theory:

$$M_c = \frac{3\rho \cdot R \cdot T}{E_{rubbery}} \quad (2)$$

where $E_{rubbery}$ is the modulus at $T=T_g + 30K$, ρ is the density (determined in a pycnometer using methanol), R is the universal gas constant (8.314 J/(K.mol)), and T is the absolute temperature. M_c is an apparent value because in the rubber nanocomposites it implies not only the crosslinking but also effects of the rubber–filler and filler–filler interactions. All the above mentioned data are tabulated in Table 3.

To characterize the filler-rubber interaction also the change in the mechanical loss factor (tanδ) can be considered. The reinforcing efficiency (R) in this case is given by [12]:

$$R = \frac{\tan\delta_{max,ref} - \tan\delta_{max}}{\tan\delta_{max,ref}} \quad (3)$$

where $\tan\delta_{max,ref}$ and $\tan\delta_{max}$ represent the peak values of the unfilled and filled rubber (nanocomposite), respectively. The larger is R, the higher is the rubber-filler interaction.

The above parameters are summarized in Table 3. Based on the data in Table 3 it can be concluded that BA acts as reinforcing nanofiller in NR. Its action, however, differs from that of traditional nanofillers (carbon black, silica) due to the fact that the T_g is slightly sifted toward lower temperature along with a small reduction of the height of the T_g peak. This is a peculiar feature that requires further investigations.

Table 3. DMA-related and Payne effect representing parameters for the NR/BA nanocomposites

Designation	T_g [°C]	tanδ max. [1]	R [1]	E'_{glassy} [MPa]	$E'_{rubbery}$ [MPa]	M_c (T_g+30°C) [g/mol]	E' at 0.01% strain (M0,01) [MPa]	Payne effect, M0,01-M10
NR ref	-43.6	2.39	0	3446	1.60	3876	1.73	0.72
NR-2.5BA	-45.9	2.30	0.038	3856	1.89	3327	2.02	0.96
NR-5BA	-46.6	2.26	0.054	3896	2.23	2855	2.54	1.04
NR-7.5BA	-46.6	2.18	0.088	3840	2.81	2311	2.95	1.39
NR-10BA	-46.8	2.12	0.113	4108	3.07	2160	3.52	1.89
NR-15BA	-46.8	2.05	0.142	4193	3.41	2015	4.75	2.43

Figure 3 displays the Payne-effect of the NR/BA nanocomposites. Note that this effect is related to the formation of a filler network [13]. The decrease in the tensile E'-modulus as a function of strain is due to a progressive destruction of the filler-filler interaction in the related nanocomposites. The Payne effect in this work was quantified by the modulus at 0.01% (M0.01), and modulus change between 0.01 and 10% (M0.01-M10) [14]. The related data are tabulated also in Table 3. It is noteworthy that M0.01 is a more sensitive parameter than M0.0.1-M10. M0.01 monotonously increased with increasing BA loadings. Practically the same information can be deduced when the M0.01-M10 data of the related nanocomposites are taken into account.

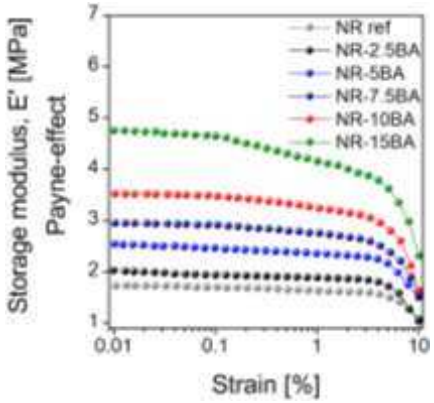

Figure 3. Storage modulus vs. strain curves measured in tension mode in DMA for the NR/BA nanocomposites

3.4. Differential scanning calorimetry

Based on the rubber-filler interaction reflecting DMA some change in the immobilized rubber layer's thickness is expected. Therefore, DSC tests were performed to estimate the amount of the immobilized rubber layer *via* [15]:

$$\Delta C_{pn} = \frac{\Delta C_p}{1-w} \tag{4}$$

$$\chi_{im} = \frac{\Delta C_{p0} - \Delta C_{pn}}{\Delta C_{p0}} \tag{5}$$

where ΔC_p is the heat capacity at the T_g jump, ΔC_{pn} is normalized to the polymer weight fraction, w is the weight fraction of filler, ΔC_{p0} is the heat capacity at T_g jump of the unfilled rubber. χ_{im} is the weight fraction of the immobilized polymer layer. Figure 4 shows characteristic DSC scans of selected NR/BA nanocomposites along with the related ΔC_p values. The DSC derived data are listed in Table 4.

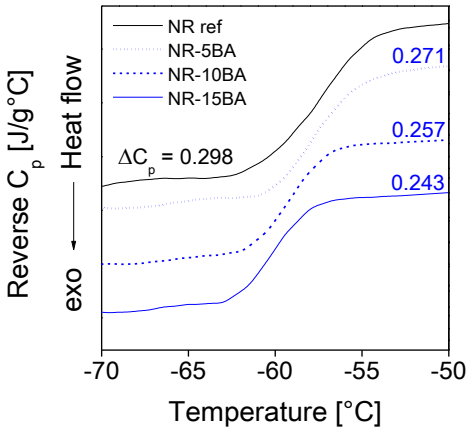

Figure 4. DSC scans in the glass transition (T_g) region of the NR and NR/BA nanocomposites containing 5, 10 and 15 phr BA amounts. Note that the Tg values deduced from DSC (cf. Figure 4) are lower than those from DMA (cf. Table 3) which is due to differences in these experiments (e.g frequency, sample amount).

Results in Table 4 are in line with the former results deduced from the DMA tests, i.e. small reduction in the height of the tanδ peak. The amount of the bound layer increased from ~5 to only ~7 wt% when the BA content was enhanced from 5 to 15 phr. This finding suggest that the BA nanoparticles worked as semi-active nanofillers.

Table 4. Heat capacity and bound layer amount for the NR/BA systems studied

Property [unit]	NRref	NR-5BA	NR-10BA	NR-15BA
Filler content [phr]	0	5	10	15
w, weight fraction [1]	0	0.043	0.083	0.120
ΔC_p, heat capacity [J/g°C]	0.298	0.271	0.2573	0.243
ΔC_{pn}, normalized heat capacity [J/g°C]	-	0.283	0.281	0.276
χ_{im}, weight fraction of the bound polymer layer [1]	-	0.049	0.058	0.074

4. Conclusions

This work devoted to study the properties of sulfur-cured natural rubber (NR)/boehmite alumina (BA) nanocomposites as a function of the BA nanofiller content. BA, being water dispersible, was mixed to the NR latex, followed by drying. These NR/BA premixes were compounded with sulfur curatives in two-roll mill before cured in a hot press.

Based on the results achieved the following conclusions can be drawn:

- BA particles were homogeneously and nanoscale dispersed in the NR/BA nanocomposites. The agglomerate size range (200-300 nm) was close to that of the in aqueous dispersion measured one (180-250 nm)
- hardness increased, whereas tensile strain decreased monotonously with increasing BA content indicating the reinforcing effect of BA. The tensile strength and the J-integral parameters related to crack imitation and propagation (J-critical and T_J, respectively) went through a maximum (peaked at about 7.5 phr) as a function of BA loading that was traced to the onset BA particles' agglomeration at higher BA contents
- DMA results indicated that with increasing BA amount both the glassy and rubbery moduli were increased. On the other hand, the peak height of the T_g-transition was only slightly reduced with

BA loading. The Payne-effect was enhanced with increasing BA loading, as expected. DSC tests indicated a small increase in the bound (immobilized) layer fraction with increased BA content. Based on these results it was concluded that unmodified BA acts as a semi-active reinforcement in NR.

Acknowledgements
This work was performed in the framework of a bilateral project between the Hungarian Academy of Science (Project number: NKM 55/2015) and Vietnam Academy of Science and Technology (VAST.HTQT.HUNGARY.01/16-17 - Institute of Chemistry), and partly also supported by the Hungarian Scientific Research Fund (OTKA 109409).

References

[1] Karger-Kocsis J, Kmetty A, Lendvai L, Drakopoulos S X and Barany T 2015 Water-Assisted Production of Thermoplastic Nanocomposites: A Review *Materials* **8** 72-95
[2] Hietala M, Mathew A P and Oksman K 2013 Bionanocomposites of thermoplastic starch and cellulose nanofibers manufactured using twin-screw extrusion *European Polymer Journal* **49** 950-6
[3] Karger-Kocsis J and Lendvai L Polymer/boehmite nanocomposites: A review *Journal of Applied Polymer Science* 45573-n/a
[4] Manek E, Berke B, Miklosi N, Sajban M, Doman A, Fukuda T, Czakkel O and Laszlo K 2016 Thermal sensitivity of carbon nanotube and graphene oxide containing responsive hydrogels *Express Polymer Letters* **10** 710-20
[5] Galimberti (Ed.) M 2011 *Rubber-Clay Nanocomposites: Science, Technology, and Applications* (Hoboken, New Jersey: Wiley)
[6] Gatos K G and Karger-Kocsis J 2010 *Rubber Nanocomposites,* ed S Thomas and R Stephen: John Wiley & Sons, Ltd) pp 169-95
[7] Varghese S and Karger-Kocsis J 2003 Natural rubber-based nanocomposites by latex compounding with layered silicates *Polymer* **44** 4921-7
[8] Wu X, Lin T F, Tang Z H, Guo B C and Huang G S 2015 Natural rubber/graphene oxide composites: Effect of sheet size on mechanical properties and strain-induced crystallization behavior *Express Polymer Letters* **9** 672-85
[9] Berki P, László K, Tung N T and Karger-Kocsis J 2017 Natural rubber/graphene oxide nanocomposites via melt and latex compounding: Comparison at very low graphene oxide content *Journal of Reinforced Plastics and Composites* **36** 808-17
[10] Florjanczyk Z, Debowski M, Wolak A, Malesa M and Plecha J 2007 Dispersions of organically modified boehmite particles and a carboxylated styrene-butadiene latix: A simple way to nanocomposites *Journal of Applied Polymer Science* **105** 80-8
[11] Ramorino G, Agnelli S, De Santis R 2010 Investigation of fracture resistance of natural rubber/clay nanocomposites by J-testing *Engineering Fracture Mechanics* **77** 1527-36
[12] Fu G J, Chang X Z, Mao J and Shi X Y 2016 Insights into the Reinforcement of Butyl Rubber by Carbon Black and Silica with the Aid of Their Dynamic Properties *Journal of Macromolecular Science Part B-Physics* **55** 925-36
[13] Roland C M 2013 *The Science and Technology of Rubber (Fourth Edition),* (Boston: Academic Press) pp 285-336
[14] Berki P, Göbl R and Karger-Kocsis J 2017 Structure and properties of styrene-butadiene rubber (SBR) with pyrolytic and industrial carbon black *Polymer Testing* **61** 404-15
[15] Zhong B C, Jia Z X, Luo Y F, Jia D M and Liu F 2017 Understanding the effect of filler shape induced immobilized rubber on the interfacial and mechanical strength of rubber composites *Polymer Testing* **58** 31-9